ACTA IMEKO
ISSN: 2221-870X
December 2024, Volume 13, Number 4, 1 - 10

Experimental and Finite Element Model-based framework for grasping force analysis with electrostatic microgrippers: a case study using a human hair

Gabriele Bocchetta[1], Giorgia Fiori[1], Federico Filippi[1], Pietro Ursi[2], Vincenzo La Battaglia[1], Stefano Marini[1], Salvatore A. Sciuto[1], Andrea Scorza[1]

[1] *Department of Industrial, Electronic and Mechanical Engineering, Roma Tre University, Via della Vasca Navale 79, 00146 Rome, Italy*
[2] *Department of General Surgery and Surgical Specialties "Paride Stefanini", Sapienza University of Rome, Viale del Policlinico 155, 00161 Rome, Italy*

ABSTRACT
Microgrippers (MGs) are MEMS devices designed specifically for microscopic-scale object manipulation, which makes them ideally suited for implementation in biomedical tissue manipulation applications. This work presents a novel method for estimating the grasping force of a MG prototype equipped with electrostatic rotary comb-drives and Conjugate Surface Flexure Hinges using a cross-approach based on both experimental and a finite element analysis. Firstly, the torque exerted by the microactuators, necessary to deform the MG has been evaluated. The rotation of the microactuators is measured in the experimental analysis through an image analysis approach developed by the Authors from videos acquired by a camera mounted on a trinocular optical microscope, while the hinge stiffness has been determined using numerical simulations. This torque provided an initial estimate of the grasping force potential. Subsequently, in order to evaluate the force that the jaws of the MG are capable of applying in grasping operations, experimental tests have been carried out on a human hair with a diameter of (86 ± 3) µm. The results obtained show that the jaws of the device apply a maximum force of (1.42 ± 0.18) µN while grasping the hair.

Section: RESEARCH PAPER

Keywords: microgripper; CSFH; grasping force; micro-manipulation; biomedical applications

Citation: G. Bocchetta, G. Fiori, F. Filippi, P. Ursi, V. La Battaglia, S. Marini, S. A. Sciuto, A. Scorza, Experimental and Finite Element Model-based framework for grasping force analysis with electrostatic microgrippers: a case study using a human hair, Acta IMEKO, vol. 13 (2024) no. 4, pp. 1-10. DOI: 10.21014/actaimeko.v13i4.1783

Section Editor: Luca Callegaro, INRiM, Italy

Received February 18, 2024; **In final form** September 6, 2024; **Published** December 2024

Corresponding author: Gabriele Bocchetta, e-mail: gabriele.bocchetta@uniroma3.it

1. INTRODUCTION

Microgrippers (MGs) are miniaturized devices that belong to the category of Micro-Electro-Mechanical Systems (MEMS). They are capable of grasping, manipulating, and releasing objects with micrometric or submicrometric dimensions [1]-[4]. Their typical size ranges from a few tens of micrometers to a few millimeters, making them suitable for interacting with objects at micro and nanoscopic scales. MGs can find applications in various fields, including microrobotics, microassembly, and biomedicine for the manipulation of cells, tissues, and microorganisms [5]-[7]. Their versatility has lately been demonstrated in operations such as versatile grasping and autonomous pick-and-place [8], [9]. MGs can be considered as miniaturized tweezers, equipped with two or more fingers capable of moving and closing to grasp objects. Their structure can be simple or complex, depending on the operating principle and specific applications. The scientific literature in the field presents several studies on MGs that use different operating principles: piezoelectric [10], [11], shape memory alloys [12], electrothermal [13], and electrostatic [14]. The latter is characterized by numerous advantages such as simplicity of design and high flexibility due to the different geometries they can have and because the materials used in their fabrication are biocompatible, which makes them suitable for use in biomedical applications [15]. Despite the numerous advantages, the literature lacks results obtained from the accurate measurement of grasping force. This type of MG utilizes electrostatic forces to move actuators, which can be characterized by different

structures: lateral [16], transverse [17], and rotary comb-drives [18]. From the literature study, the latter structure has been shown to be the type of actuator with the highest efficiency, i.e., the ratio between displacement and supply voltage [14], [19]-[27]. There are several solutions for rotary microactuators, which require a hinge for the relative motion of the movable comb with respect to the fixed one. In the scientific literature some studies propose a simple linear flexure beam that acts as a hinge [22], [23]. The solution above is the simplest to design and fabricate but it also has the drawback of producing instability in the rotation. This is because as the supply voltage increases, the comb-drive fingers approach each other transversally, which could lead to microactuator failure.

Alternative solutions feature freeform geometries for the flexure beams [27]. This type of beam, with the same actuation voltage and radius of rotation, i.e., the distance between the rotation centre and comb-drive fingers, exhibits significantly greater displacement compared to straight beams. However, a downside is that the transverse displacement of the fingers is also accentuated. In [28], it has been demonstrated that the flexure beam geometry that most closely approximates the ideal rotation is the circular geometry, in which the centre of rotation of the microactuator corresponds to the centre of the elastic weights of the beam. In the circular geometry, with the same dimensions as liner beams and actuation voltage, the displacement they produce is compatible, but the transverse displacement is reduced.

Based on these considerations, the MG prototype exanimated in the present study is equipped with Conjugate Surface Flexure Hinges (CSFHs) [29]-[31]. Figure 1a shows a schematic of the Device Under Test (DUT), while Figure 1b shows a detail of a portion of the MG, in which part of the electrostatic microactuator and the CSFH are captured by an optical microscope. The structure features a pair of CSFHs and is actuated by a pair of rotary comb-drives.

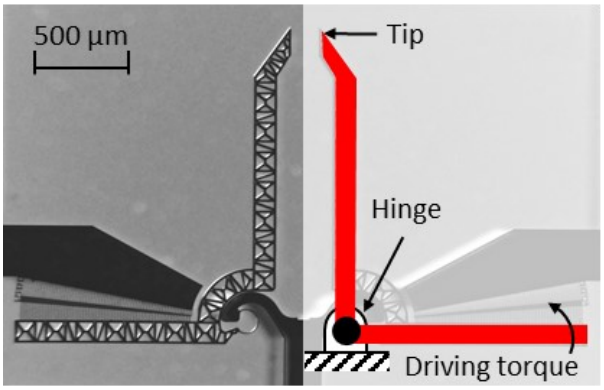

(a)

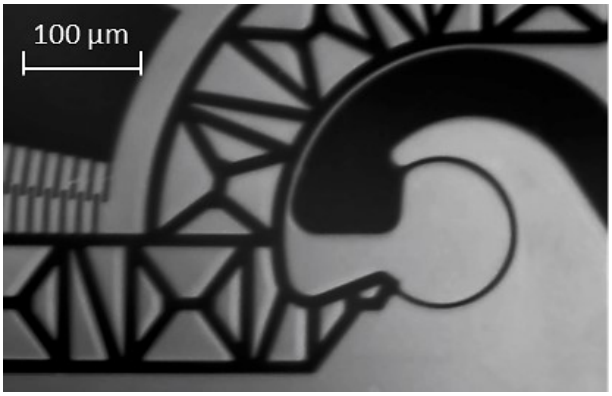

(b)

Figure 1. Microgripper images captured by optical microscope: (a) entire device with a schematic of the structure and (b) detail of the comb-drive and CSFH.

Recent studies have shown that the total number of CSFHs is proportional to the energy necessary to deform the device structure. As a result, MGs with only one CSFH pair and one pair of electrostatic rotary-comb drives [32] demonstrated a wider range of displacement considering the same applied voltage than MGs composed of a double four-bar linkage with multiple CSFHs [33] and that the displacement is proportional to the number of microactuators [34]. On the other hand, the trajectory of the jaws is not linear but follows a circumferential arc as opposed to four-bar linkage-based devices.

In this context, the present work focuses on a CSFH-based MG equipped with only one CSFH pair, with the aim to investigate the mechanical behaviour of the hinges through experimental analysis, and Finite Element Analysis (FEA). In particular, the torque exerted to deform the flexure hinges and the grasping force in manipulation tasks have been estimated.

The torque has been evaluated by a cross-approach based on experimental image analysis [35], and finite element analysis [36]. The experimental analysis has been carried out through the analysis of images obtained from an optical microscope equipped with a high-resolution camera and a measurement procedure developed *ad hoc* by the authors in MATLAB environment to evaluate the kinematic characteristics of the device. In particular, the angular displacement of the comb-drives and gripper tips have been evaluated as a function of supply voltage values. These results have been considered as a reference for numerical simulations that have been used to evaluate the stiffness coefficient of the curved beams of the CSFHs. This analysis is mandatory to estimate the force that the microgripper is able to apply on a manipulated object. This issue is critical for ensuring precision and safety during micromanipulation operations, as torque assessment allows for the measurement of force between the two MG jaws [37]. In the present work, human hair has been used as the object to grasp [38].

The present work is organized as follows. Section 2 describes the components of the experimental setup, their main characteristics, and the main steps of the displacement evaluation through image processing and numerical simulations, both for the preliminary analysis for the torque assessment and the estimation of the grasping force using the hair. In Section 3 the analysis of the uncertainties involved during the experimental tests has been carried out, while Section 4 presents the results obtained from the estimation of the torque and grasping force. Finally, in Section 5 a summary of the findings and directions for future research is reported.

2. MATERIALS AND METHODS

The DUT is a rotary comb-drive actuated MG prototype equipped with CSFHs [39], [40] that has been fabricated monolithically by the Deep Reactive Ion Etching (DRIE) process on SOI (Silicon-On-Insulator) wafer with a rigid aluminium mask [41]-[43]. The main geometrical characteristics of the device are listed in Table 1.

To evaluate the grasping force, a kinematic characterization of the device has been first performed, measuring the displacements that the MG is able to achieve as a function of the supply voltage, when it does not perform manipulation operations and the jaws are free to move.

Table 1. Microgripper main design specifications.

Component		Symbol	Value
SOI Wafer	Device layer thickness	b	40 µm
	Buried oxide layer thickness		5 µm
	Handle layer thickness		400 µm
CSFH	Number of CSFH		2
	Curved beam length		252 µm
	Curved beam width	h	5 µm
	Neutral axis curvature radius	r_n	62.5 µm
	Curved beam subtended angle	α	240.9°
	Conjugate surfaces clearance		2 µm
Comb-drive	Number of fingers per comb-drive		64
	Finger distance		10 µm
	Rotor-Stator finger distance		3 µm
	Finger width		4 µm
	Finger minimum length		38 µm
	Finger maximum length		151 µm
	Initial overlapping angle		2°

Several experiments have been conducted to determine the angular displacement of the comb-drive. In particular, videos of the DUT have been acquired through a trinocular optical microscope fitted with a video camera at different magnification levels [44]. The videos have been processed using a MATLAB-developed measurement procedure [32], [33]. The experimental analysis aims to measure the actual angular displacement of the microactuator, while FEA can be used to estimate the stiffness coefficient of the curved beam. From the angular displacement and the stiffness of the CSFH the torque required by the actuator to deform the structure is evaluated. A finite element model has been implemented in COMSOL Multiphysics by numerically

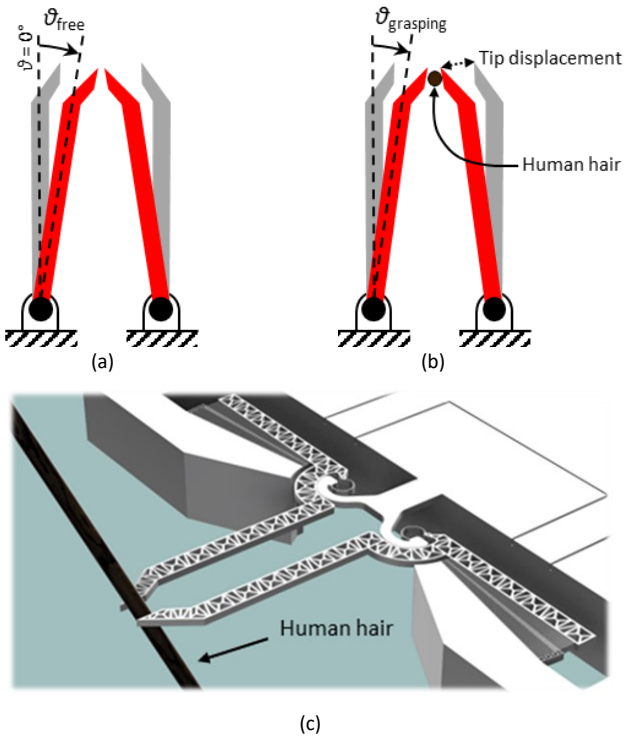

Figure 2. Schematization of test conditions: (a) MG free to move, to evaluate the comb-drives angular displacement ϑ_{free}, (b) MG performing hair grasping in which tip displacement and rotation $\vartheta_{grasping}$ are measured. (c) 3D rendering of the hair grasping test.

Table 2. Experimental setup main components.

Device	Characteristics
Arbitrary/Function Generator	Amplitude: 0 to ± 10 V peak-to-peak, Frequency: 0.01 µHz to 5 MHz
Power amplifier	Amplitude: 0 to ± 20 V
DC power supply	Voltage: 0 to 30 V Resolution: 1 mV
Light microscope	Zoom: 16×, 20×, 40×, 60×, 80×, 100×
Micropositioners	Travel range (X/Y/Z): 10 mm Screw resolution (X/Y/Z): 500 µm
Video camera	23.3 MP, sensor size ½.3 in, maximum video resolution, and fps: 4K (3840 × 2160 pixel) at 120 fps
Video Processing software	In-house algorithm implemented in MATLAB (2022b, MathWorks)
PC	Intel® Core i7-11370H, 32 GB RAM, NVIDIA® RTX™ 3050 Ti

simulating the angular displacement of the microactuator as a function of the electric potential to evaluate the stiffness coefficient. The outcomes of the experimental phase served as the starting point for the numerical simulations that have been performed. This has made it possible to evaluate the CSFH's stiffness taking into consideration the same comb-drive rotation and the supply voltage used for the experimental actuation of the DUT.

Finally, to provide an example of grasping force assessment in operational conditions, some experimental tests have been conducted on a human hair: once the contact between the jaws and the hair occurred, the displacement values have been assessed necessary to evaluate the resisting torque, while for the driving torque, the values previously obtained for each supply voltage value have been used. Figure 2 shows a schematic of the test conditions in which the MG can move freely and in which it performs hair grasping. Figure 2a shows the test condition in which the MG is free to move and in which the displacements of the main components, i.e., tip displacement and comb-drive rotation (ϑ_{free}) have been evaluated. Similarly, Figure 2b shows the test condition in which the MG performs hair grasping and in which the tip displacement, up to the hair contact, and the angular displacement of the microactuators ($\vartheta_{grasping}$) have been evaluated.

2.1. Kinematic characterization

The angular displacement of the microactuators has been determined by processing videos obtained using a high-resolution and framerate camera installed on a trinocular optical microscope. Different magnification levels have been set to acquire both the CSFH and the free end of the comb-drive at 80×, and the entire comb-drive at 40×.

The power instrumentation, which consisted of a function generator, a power amplifier, and micropositioners for positioning tungsten needles that power the MG via contact, as well as the image acquisition instrumentation [44], which consists of a trinocular optical microscope with a video camera, comprise the experimental setup used to carry out the experimental testing of the DUT. The main components' specifications are summarized in Table 2. A trapezoidal ramp signal with a peak-to-peak amplitude between 0 and 20 V and a period of 2 s has been set into the power instrumentation. This kind of waveform as a power signal ensures that the DUT has a phase in which it remains stationary in both the neutral and maximum

displacement positions. Acquired videos were long enough to capture at least 30 periods of the power signal.

Data has been processed and analysed through a measurement procedure developed in MATLAB to estimate displacements of regions of interest via video tracking of virtual markers identified by SURF features detection [45].

Conversely, in order to measure the displacement required to grasp the hair, a manual sweep of the supply voltage has been applied using a DC power supply in the range of 0-27 V, with a step of 1 V. The actuation voltage value is due to the fact that already at 27 V a closure of the jaws is reached sufficient to grasp a hair and to remain below the pull-in voltage which has been estimated above 28 V [46]. Subsequently, the acquired image series have been processed with the abovementioned virtual marker tracking procedure.

2.2. Curved beam stiffness estimation

Numerical simulations have been carried out using COMSOL Multiphysics software. To minimize computational costs, FEA simulations have been conducted using the MG's bidimensional model, to which an out-of-plane thickness of 40 μm has been applied. In particular, the CAD drawing used to make the aluminium hard mask during the fabrication process constituted the source of the 2D model for numerical simulations. To this aim, both the Solid Mechanics and the Electrostatics modules have been included. The first has been used to simulate the deformation of the structure and especially the CSFHs, while the second one to reproduce the actual MG operating principle and to model the electrostatic forces involved.

The air surrounding the DUT as a free-deforming domain has been included in the numerical model to make the simulation of the comb-drive electrostatic actuation even more realistic. In addition, to capture the intricacies of the comb-drive micro-features and air interaction, the mesh has been optimized, and considering large deflections, non-linear effects have been included. The numerical model used <100> silicon as the device material, matching the real-world prototype, and the Young's modulus has been set in line with the values in [47]-[49].

The stiffness coefficient k can be estimated as a first approximation by considering CSFHs as homogeneous, linear elastic beams with uniform, rectangular cross sections and assuming the bending moment to be constant [50], [51]:

$$k \cong \frac{1}{12}\frac{E\, b\, h^3}{r_n\, \alpha}, \tag{1}$$

where E is Young's modulus of the silicon, b indicates the device thickness, while h is the curved beam width, r_n is the neutral axis curvature radius, and α is the subtended angle by the latter.

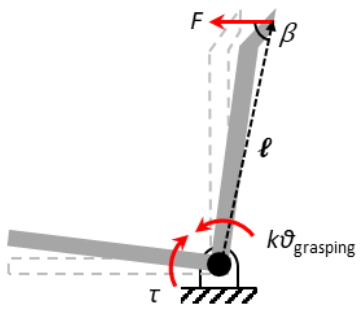

Figure 3. Schematization of the system of forces and torques present during the grasping tests.

2.3. Grasping force analysis

Since in the first phase of experimental tests, the DUT could move freely, i.e., it did not perform any manipulation operation, each position reached by the MG can be considered as an equilibrium condition between the torque exerted by the electrostatic actuator and the resistant torque due to the elastic behaviour of the CSFH. In this way, the actuation torque (τ) can be evaluated as:

$$\tau = k\, \vartheta_{\text{free}}, \tag{2}$$

where k and ϑ_{free} indicate the stiffness coefficient of the CSFH and the microactuator angular displacement, respectively.

In order to assess the grasping force, it can be considered the condition shown in Figure 3. By observing the electrostatic torque that the actuator can apply and the resisting torque of the hinge, the following relationship can be considered:

$$\tau = k\, \vartheta_{\text{grasping}} + F\, \ell \sin\beta, \tag{3}$$

where $\vartheta_{\text{grasping}}$ indicates the comb-drive rotation when the MG grasps the hair, F is the force due to the interaction between the jaw and hair, ℓ is the arm length between the point of force application and the centre of rotation, and β indicates the subtended angle. Therefore, the force applied by the individual jaw can be evaluated as:

$$F = \frac{\tau - k\, \vartheta_{\text{grasping}}}{\ell \sin\beta}. \tag{4}$$

The total grasping force will be given by the sum of the forces applied by both jaws.

Furthermore, by using the finite element model implemented to estimate the stiffness coefficient of the curved beams of the CSFH, it is also possible to simulate hair grasping tests to estimate the increase of the Maximum Principal Stress (MPS) during grasping.

3. UNCERTAINTY ANALYSIS

Various contributions have been taken into consideration in the measurement uncertainty analysis. First, the main sources of uncertainty involving the experimental approach have been identified, and the components of these sources, i.e., type A and type B uncertainties, have been combined in quadrature and given as standard deviations (SDs) [52]. Specifically, the dispersion of the experimental results has been used to estimate type A uncertainties, whilst the instrumentation specifications have been used to estimate type B uncertainties, which are listed in Table 3.

In this respect, the optical system's uncertainty takes into account the contributions of both the spatial resolution and the

Table 3. Main uncertainty sources in the experimental approach.

Source of Uncertainty	Value
Function generator amplitude	± (1 % of $V_{\text{peak-to-peak}}$ + 2 mV)
Function generator frequency	± (3 ppm of setting + 2 pHz) Aging rate: ±1 ppm/year
Power amplifier amplitude	± 2 mV
DC power supply	± (0.03 % of RDG + 10 digits)
Optical system	± 1 μm
Maximum angular displacement uncertainty with video tracking measurement procedure	± 0.01°
Maximum tip displacement uncertainty with video tracking measurement procedure	± 0.5 μm

conversion factor of pixel size [53]. Similarly to [54]-[56], a Monte Carlo Simulation (MCS) with 10^4 iterations for the MG prototype has been carried out to assess the uncertainty associated with comb-drive angular displacement and the gripper tip displacement measuring process.

The virtual markers' centroid position has been made to vary randomly in the image through the inclusion of different markers during the video tracking at each MCS iteration. Moreover, the uncertainty related to FEA-derived outcomes has been quantified by means of an additional MCS with 10^4 iterations that varied the MG geometric dimensions considering the uncertainty contribution related to the DRIE process. Several variables, such as the DRIE process parameters, the wafer's material characteristics, and the measuring technique employed, might affect the dimensional uncertainty associated with the DRIE process of a SOI wafer with a 40 µm device thickness. For small elements, e.g., less than 100 µm, dimensional uncertainty in DRIE processes typically ranges from 1 % to 5 % of the element size [57]-[60]. This would correspond to an uncertainty that can vary from a few tens of nanometres to a few hundred nanometres for a 5 µm feature, i.e., the width of the CSFH's flexure beam.

The thickness-related uncertainty has been assessed through several measurements on an image of the hair obtained under an optical microscope. The contribution related to the position of the hair between the MG jaws has been estimated by taking into account the distance between the MG tips in the case of maximum jaw closure during the grasping tests.

Finally, the measurement uncertainty of the grasping force has been determined by means of the error propagation law applied to (4), taking into account the standard uncertainties associated with the stiffness coefficient, the geometrical dimensions of the DUT and the angular displacements.

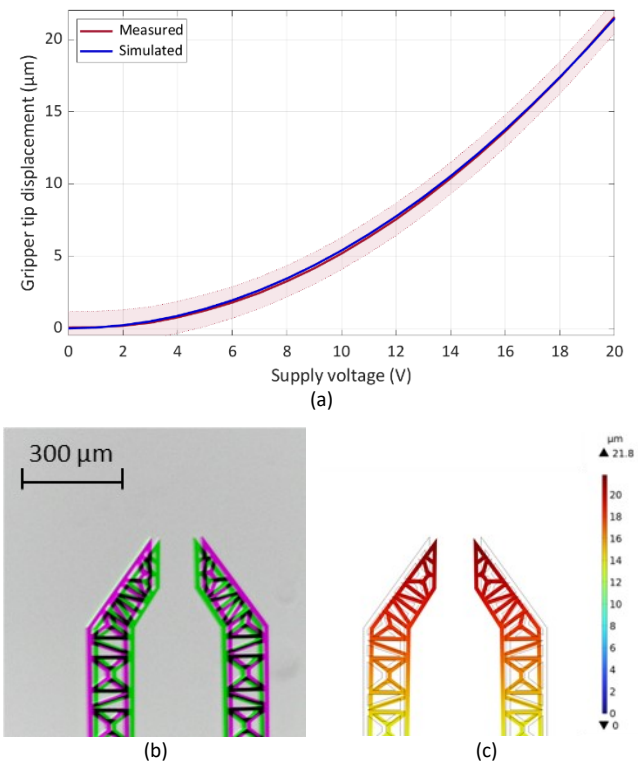

Figure 4. Measured and simulated tip displacement: (a) displacement as a function of the supply voltage and comparison of 0 V and 20 V positions evaluated by (b) experimental approach (neutral position in magenta, displacement at 20 V in green) and (c) FEA.

4. RESULTS AND DISCUSSION

This section presents and discusses the outcomes of the experimental tests related to the angular displacement of the MG comb-drives and the gripper tip displacements as a function of the supply voltage and the results from numerical simulations, including the hinge stiffness coefficient. Furthermore, the results of grasping force are presented. The results are expressed in terms of the mean value ± SD.

Preliminary results obtained from the processing of the videos acquired during the experimental tests show a maximum rotation of the comb-drives of 0.80° ± 0.01° at 20 V, which corresponds to a maximum tip displacement of (22.1 ± 1.1) µm. Numerical simulations performed to estimate the beam stiffness coefficient show a maximum angular displacement of the comb-drives of 0.79° and a tip displacement of 21.8 µm at 20 V, respectively. Figure 4a shows the trend of tip displacement as a function of supply voltage (in the range 0-20 V), evaluated both experimentally and through numerical simulations. Moreover, an example of the tip positions for two different supply voltages is shown in Figure 4b and 4c for the experimental and FEA outcomes, respectively.

Based on the angular displacement outcomes, the stiffness coefficient of the CSFH curved beam has been calculated to be (0.10 ± 0.01) µN·m·rad^{-1}, through the numerical analysis performed by simulating the electrostatic and the results

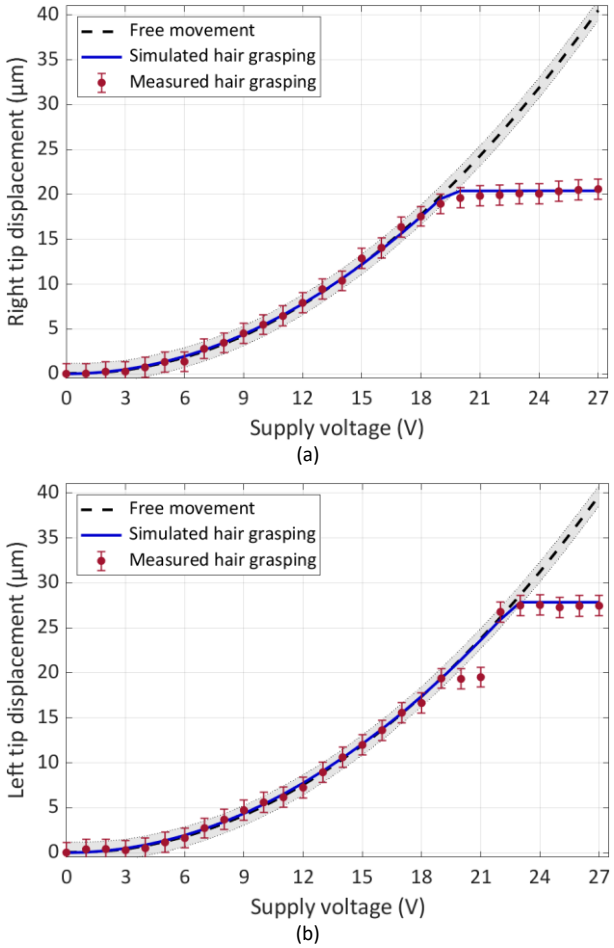

Figure 5. Displacement of the MG tips as a function of the supply voltage: (a) right tip and (b) left tip. Comparison between displacements obtained with the gripper free to move (dashed black line) and the results obtained experimentally (red dots) and from numerical simulations (blue line) from the hair gripping test.

obtained by the torque assessment are in agreement with what has been reported in the literature both in terms of trend and order of magnitude [61].

Afterward, the displacement of the comb-drives and tips of the DUT has been measured by means of a manual voltage sweep in the range of 0-27 V, with a 1 V-step using a DC power supply, in order to compare the behaviour as a function of supply voltage between the test conditions in which the MG moves freely without performing manipulation operations and in which it grasps the hair.

The results obtained for the first test condition, i.e., MG free to move, show that at 27 V the left comb-drive rotates by 1.48° ± 0.01° experimentally and 1.45° from numerical simulations. This rotation corresponds to a maximum left tip displacement of (40.5 ± 1.1) µm obtained experimentally and a simulated displacement of 39.6 µm. Similarly, the experimentally measured maximum rotation of the right comb-drive is 1.45° ± 0.01° and 1.44° simulated, which corresponds to a right tip displacement of (39.7 ± 1.1) µm measured and 39.5 µm simulated.

During the hair grasping tests, the results obtained show that the maximum displacement decreases to the point of stopping at the moment when both jaws come into contact with the hair. In particular, regarding the right half of the DUT, which is the first to come into contact with the hair since it is not centred between the jaws, the comb-drive stops at a maximum angular displacement of 0.75° ± 0.01°, which corresponds to a tip displacement of (20.6 ± 1.1) µm. Figure 5a shows the trend of the right tip as a function of supply voltage both in the test condition where it is free to move and in the presence of the hair. From the latter can be observed that once a certain voltage value is reached, around 20 V, which corresponds to the contact between the right jaw and hair, the displacement stops increasing with increasing supply voltage.

Moving on to the other half of the DUT, the behaviour is dual, and the left comb-drive rotates up to a maximum of 1.01° ± 0.01°, which causes the left jaw to move a maximum of (27.5 ± 1.1) µm. As in the previous case, Figure 5b shows the evolution of the left tip under free conditions and during grasping. However, from the experimental results obtained for the displacement of the left tip, as can be seen in Figure 5b, some displacement values obtained from the results do not follow the quadratic trend as a function of the supply voltage. The most probable cause may be attributed to the fact that the hair, in addition to not being centred between the jaws, is also not perpendicular to them. In fact, if we consider the nominal value of the jaw opening of 150 µm and the maximum jaw displacement, a closure of (101.9 ± 2.2) µm has been determined. Since a diameter of (86 ± 3) µm has been measured, it is possible to hypothesize that the hair is tilted by about 32.5° ± 0.2° with respect to the vertical, and this causes the upper edge of the left jaw to be the first to come into contact with the hair. On the other hand, the edge of the right jaw comes into contact with the hair at around 19 V when the tip moves by (19.4 ± 1.1) µm. Subsequently, as the supply voltage increases, the tip does not move until it reaches a value of around 22 V, at which voltage value the gripper is able to apply enough force to move the hair and thus continue closing the jaw until the hair is grasped at around 23 V when the tip reaches its maximum displacement value of (27.5 ± 1.1) µm. Figure 6 shows the initial (0 V) and final (27 V) phases of the hair grasping test.

The aforementioned findings on the size and position of the hair have been also useful for the implementation of numerical

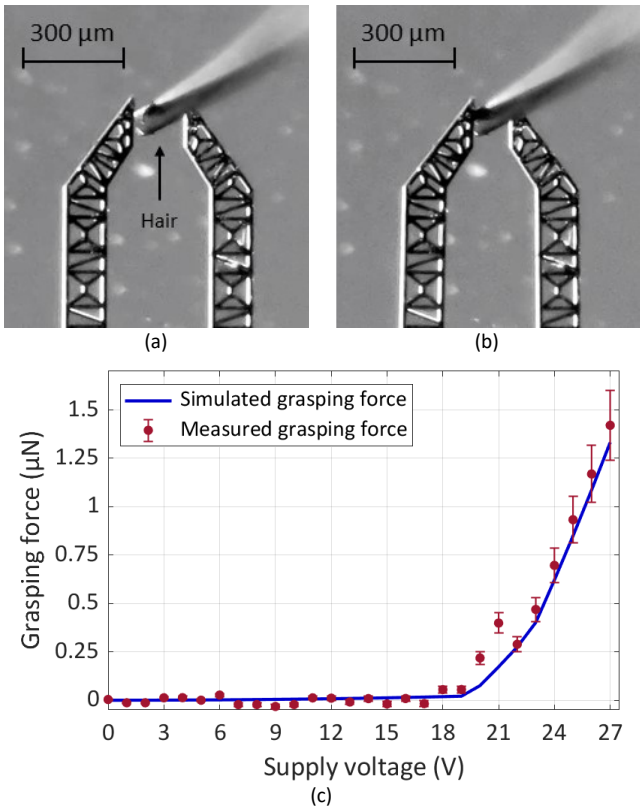

Figure 6. Hair Grasping Test: (a) neutral jaw position at 0 V; (b) maximum closure position obtained for the maximum considered voltage value (27 V); (c) trend of experimental and simulated grasping force results as a function of the supply voltage.

Table 4. Summary of maximum values. Experimental data are expressed as mean value ± standard deviation.

Parameter		Value	
CSFH Stiffness coefficient (µN·m·rad^{-1})		0.10 ± 0.01	
		Left	**Right**
Free movement	Measured comb-drive maximum angular displacement (°)	1.48 ± 0.01	1.45 ± 0.01
	Simulated comb-drive maximum angular displacement (°)	1.45	1.44
	Measured gripper tip maximum displacement (µm)	40.5 ± 1.1	39.7 ± 1.1
	Simulated gripper tip maximum displacement (µm)	39.6	39.5
	Maximum CSFH principal stress principal stress corresponding to hair contact (MPa)	12.26	8.99
Grasping test	Measured comb-drive maximum angular displacement (°)	1.01 ± 0.01	0.75 ± 0.01
	Simulated comb-drive maximum angular displacement (°)	1.02	0.74
	Measured gripper tip maximum displacement (µm)	27.5 ± 1.1	20.6 ± 1.1
	Simulated gripper tip maximum displacement (µm)	27.8	20.4
	Maximum CSFH principal stress principal stress corresponding to hair contact (MPa)	12.51	9.40
Maximum grasping force (µN)		1.42 ± 0.18	

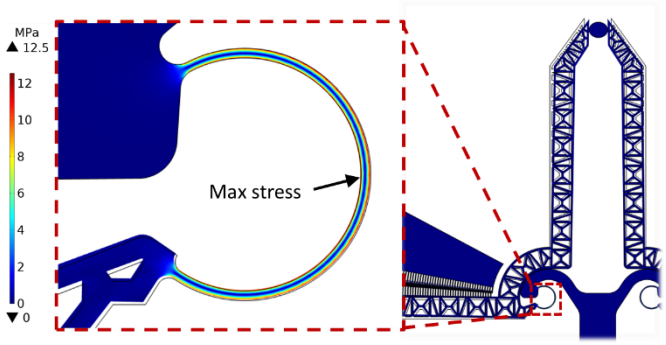

Figure 7. Stress contour plot for the left CSFH according to FEA by simulating hair grasping.

simulations on the hair grasping test using the DUT finite element model. This allowed to replicate the tip displacements obtained by the MG and to numerically estimate the grasping force and the MPS increment of CSFHs. To simulate the grasping of the tilted hair, an elliptical cross-section has been considered and the mechanical properties have been chosen according to [62], [63].

Figure 6c depicts the trend of the grasping force as a function of the supply voltage, both for the experimental results and those obtained through numerical simulations. The results have been obtained by considering (4) for all DUT supply voltage values considered in the present study. As long as the MG jaws move freely, the electrostatic torque equals the resisting torque of the CSFHs. When contact with the hair occurs (Figure 3), the resisting torque becomes smaller than the driving torque because, at the same voltage, the displacement produced by the MG is smaller than what would be obtained without hair. This difference in torque results into a force that the jaw applies on the hair, up to the final value of supply voltage that corresponds to a maximum grasping force of (1.42 ± 0.18) μN. Table 4 summarizes the maximum values of the results obtained from experimental tests and FEA.

Finally, as for the MPS analysis of the CSFHs, the value obtained by simulating the free movement of the DUT at the angular displacement value corresponding to hair contact has been considered, i.e., 0.74° at 20 V and 1.02° at 23 V for the left and right comb-drives, respectively. The simulation results show a MPS of the left and right CSFHs of 12.26 MPa and 8.99 MPa, respectively. In both cases, the stress is two orders of magnitude lower than the yield stress (6.9 GPa), and both beams' rupture is prevented. By simulating the hair grasping, the displacement of the tips does not increase because they are in contact with the hair without deforming it, therefore the increase in grasping force results in an increase in MPS for the CSFHs. In particular, the previously obtained MPS values increase to 12.51 MPa and 9.40 MPa, which correspond to a percentage increase in MPS of about 2 % for the left CSFH and 4 % for the right CSFH. Figure 7 shows the stress contour plot for the left CSFH, the one that is most deformed when the MG grasps the hair. The left hinge reaches a higher MPS because it is the one that deforms the most, but on the other hand, the right hinge has a higher percentage increase of MPS since, at the same tip position, it is subjected to a greater increase in the force it applies on the hair.

5. CONCLUSIONS

The study presented a novel method for estimating the grasping force applied by the jaws of a MEMS microgripper for biomedical applications. The results obtained in this study demonstrated the effectiveness of the combined experimental and finite element approach proposed for the kinematic characterization of the device and the estimation of the torque exerted by the actuators of the device. In particular, the experimental results, obtained by processing images and videos of the DUT through an *ad hoc* measurement procedure in MATLAB environment, allowed to measure both the angular displacement of the microactuators and the displacement of the tips. Data have been acquired through a trinocular optical microscope equipped with a high-resolution camera and framerate. The results concerning the comb-drive rotation have been used to estimate the stiffness coefficient of the curved beam of the CSFH through numerical simulations with the element analysis implemented in COMSOL Multiphysics. From the results obtained, the stiffness coefficient of the curved beams of CSFHs has been estimated to be (0.10 ± 0.01) μN·m·rad^{-1}. This value has been subsequently used to estimate the torque applied by the rotary electrostatic microactuators. The driving torque analysis is necessary to estimate the grasping force that the MG is capable to apply during experimental tests of grasping a human hair. In order to estimate the grasping force, the displacement of the main components of the DUT, i.e., comb-drives and tips, during free movement and with the hair placed between the jaws has been considered. The difference obtained from the displacement results is reflected in a difference in torque that the microactuators are able to apply at the same displacement. In particular, a maximum grasping force of (1.42 ± 0.18) μN has been estimated at 27 V, considered as the maximum value for MG actuation due to the pull-in phenomenon.

The results obtained in this study represent a first step forward in the development of assessment methods for the force applied by rotary electrostatic microactuators actuated MG. Through the finite element model implemented for the characterization of CSFHs, hair grasping tests have been performed to simulate the experimentally obtained force values, with the aim of analysing the trend of the MPS as the applied force increases. However, the values obtained are two orders of magnitude lower than the critical value for silicon. Moreover, further experimental tests conducted on different devices could validate the mathematical model, allowing the implementation of a phy-digital twin of the device that can be used to simulate the behaviour of the system under conditions different from those of the experiments. In this scenario, applications of MGs, including the behaviour of microactuators when manipulating objects with different sizes and shapes, can be simulated using the phy-digital twin [64]. This could make it easier to estimate, predict, and establish the optimal conditions of operation for microgrippers. The implementation of the phy-digital twin could also be useful for the development and optimization of new and more complex designs.

In the near future, it will be important to extend the method to MGs with more different geometries and apply it to nanoscale devices as well. Finally, a further aspect of fundamental interest concerns the improvement of the experimental setup, e.g., adding a second microscope with an orthogonal view for the measurement of the actual position and inclination of the object to be grasped (such as the hair in the present study) and the implementation of an experimental method for measuring the force applied by the MG with specially designed sensors. In this way, it would be possible to directly assess the force that MG jaws can apply when performing microscale tasks, such as grasping an object.

REFERENCES

[1] F. A. Mohd Ghazali, M. N. Hasan, T. Rehman, M. Nafea, M. S. Mohamed Ali, K. Takahata, MEMS actuators for biomedical applications: a review, J. Micromech. Microeng. 30 (2020). DOI: 10.1088/1361-6439/ab8832

[2] C. Chircov, A. M. Grumezescu, Microelectromechanical Systems (MEMS) for Biomedical Applications, Micromachines 13 (2022). DOI: 10.3390/mi13020164

[3] S. Bhansali, A. Vasudev (editors), MEMS for Biomedical Applications, Woodhead Publishing, Oxford, 2012, ISBN 9780857096272.

[4] G. Bocchetta, G. Fiori, S. A. Sciuto, A. Scorza, Performance of Smart Materials-Based Instrumentation for Force Measurements in Biomedical Applications: A Methodological Review, Actuators 12 (2023). DOI: 10.3390/ACT12070261

[5] Z. Zhang, X. Wang, J. Liu, C. Dai, Y. Sun, Robotic Micromanipulation: Fundamentals and Applications, Annu. Rev. Control Robot. Auton. Syst. 2 (2019), pp. 181-203. DOI: 10.1146/annurev-control-053018-023755

[6] S. Chowdhury, A. Thakur, P. Švec, C. Wang, W. Losert and S. K. Gupta, Automated Manipulation of Biological Cells Using Gripper Formations Controlled By Optical Tweezers, IEEE Trans. Autom. Sci. Eng. 11 (2014), pp. 338-347. DOI: 10.1109/TASE.2013.2272512

[7] N. Chronis and L. P. Lee, Electrothermally activated SU-8 microgripper for single cell manipulation in solution, J. Microelectromech. Syst. 14 (2004), pp. 857-863. DOI: 10.1109/JMEMS.2005.845445

[8] J. Zhang, O. Onaizah, K. Middleton, L. You and E. Diller, Reliable Grasping of Three-Dimensional Untethered Mobile Magnetic Microgripper for Autonomous Pick-and-Place, IEEE Robot. Autom. Lett. 2 (2017), pp. 835-840. DOI: 10.1109/LRA.2017.2657879

[9] T. Nishimura, Y. Fujihira, T. Watanabe, Microgripper-Embedded Fluid Fingertip-Enhancing Positioning and Holding Abilities for Versatile Grasping, J. Mech. Robot. 9 (2017). DOI: 10.1115/1.4038217

[10] Z. Lyu, Q. Xu, Novel design of a piezoelectrically actuated compliant microgripper with high area-usage efficiency, Precis. Eng. 76 (2022), pp. 1-11. DOI: 10.1016/j.precisioneng.2022.03.003

[11] Z. Lyu, Q. Xu, Recent design and development of piezoelectric-actuated compliant microgrippers: A review, Sens. Actuators A Phys. 331 (2021). DOI: 10.1016/j.sna.2021.113002

[12] A. Shelyakov, N. Sitnikov, K. Borodako, V. Koledov, I. Khabibullina, S. von Gratowski, Design of microgrippers based on amorphous-crystalline TiNiCu alloy with two-way shape memory, J. Micro-Bio Robot. 16 (2020), pp. 43-51. DOI: 10.1007/s12213-020-00126-3

[13] H. M. Fard-Vatan, M. Hamedi, Design, analysis and fabrication of a novel hybrid electrothermal microgripper in microassembly cell, Microelectron. Eng. 231 (2020). DOI: 10.1016/j.mee.2020.111374

[14] F. Beyeler, A. Neild, S. Oberti, D. J. Bell, Y. Sun, J. Dual, B. J. Nelson, Monolithically Fabricated Microgripper With Integrated Force Sensor for Manipulating Microobjects and Biological Cells Aligned in an Ultrasonic Field, J. Microelectromech. Syst. 16 (2007), pp. 7-15. DOI: 10.1109/JMEMS.2006.885853

[15] S. Yang, Q. Xu, A review on actuation and sensing techniques for MEMS-based microgrippers, J. Micro-Bio Robot. 13 (2017), pp. 1-14. DOI: 10.1007/s12213-017-0098-2

[16] C. Chen, C. Lee, Y. J. Lai, W. Chen, Development and application of lateral comb-drive actuator, Jpn J. Appl. Phys. 42 (2003). DOI: 10.1143/JJAP.42.4059

[17] Y. Sun, B. J. Nelson, D.P. Potasek, E. Enikov, A bulk microfabricated multi-axis capacitive cellular force sensor using transverse comb drives, J. Micromech. Microeng. 12 (2002). DOI: 10.1088/0960-1317/12/6/314

[18] L. A. Velosa-Moncada, L. A. Aguilera-Cortés, M. A. González-Palacios, J. P. Raskin, A. L. Herrera-May, Design of a novel MEMS microgripper with rotatory electrostatic comb-drive actuators for biomedical applications, Sensors 18 (2018). DOI: 10.3390/s18051664

[19] B. E. Volland, H. Heerlein, I. W. Rangelow, Electrostatically driven microgripper, Microelectron. Eng. 61 (2002), pp. 1015-1023. DOI: 10.1016/S0167-9317(02)00461-6

[20] T. Chen, L. Sun, L. Chen, W. Rong, X. Li, A hybrid-type electrostatically driven microgripper with an integrated vacuum tool. Sens. Actuators A Phys. 158 (2010), pp. 320-327. DOI: 10.1016/j.sna.2010.01.001

[21] S. A. Bazaz, F. Khan, R. I. Shakoor, Design, simulation and testing of electrostatic SOI MUMPs based microgripper integrated with capacitive contact sensor, Sens. Actuators A Phys. 167 (2011), pp. 44-53. DOI: 10.1016/j.sna.2010.12.003

[22] H. Chang, H. Zhao, F. Ye, G. Yuan, J. Xie, M. Kraft, W. Yuan, A rotary comb-actuated microgripper with a large displacement range, Microsyst. Technol. 20 (2014), pp. 119-126. DOI: 10.1007/s00542-013-1737-8

[23] B. Piriyanont, A. G. Fowler, S. O. Reza Moheimani, Force-controlled MEMS rotary microgripper, J. Microelectromech. Syst. 24 (2015), pp. 1164-1172. DOI: 10.1109/JMEMS.2015.2388539

[24] Q. Xu, Precision Position/Force Interaction Control of a Piezoelectric Multimorph Microgripper for Microassembly, IEEE Trans. Autom. Sci. Eng. 10 (2013), pp. 503-514. DOI: 10.1109/TASE.2013.2239288

[25] Y. Hao, W. Yuan, H. Zhang, H. Kang, H. Chang, H, A rotary microgripper with locking function via a ratchet mechanism, J. Micromech. Microeng. 26 (2015). DOI: 10.1088/0960-1317/26/1/015008

[26] R. Crescenzi, M. Balucani, N. P. Belfiore, Operational characterization of CSFH MEMS technology based hinges, J. Micromech. Microeng. 28 (2018). DOI: 10.1088/1361-6439/aaaf31

[27] C. Wang, Y. Wang, W. Fang, X. Song, A. Quan, M. Gidts, H. Zhang, H. Liu, J. Bai, S. Sadeghpour, M. Kraft, Design of a large-range rotary microgripper with freeform geometries using a genetic algorithm, Microsyst. Nanoeng. 8 (2022). DOI: 10.1038/s41378-021-00336-0

[28] A. Buzzin, L. Giannini, G. Bocchetta, A. Notargiacomo, E. Giovine, A. Scorza, R. Asquini, G. de Cesare, N. P. Belfiore, On the Dependency of the Electromechanical Response of Rotary MEMS/NEMS on Their Embedded Flexure Hinges' Geometry, Micromachines 14 (2023). DOI: 10.3390/mi14122229

[29] M. Verotti, R. Crescenzi, M. Balucani, N. P. Belfiore, MEMS-Based Conjugate Surfaces Flexure Hinge, ASME. J. Mech. Des. 137 (2015). DOI: 10.1115/1.4028791

[30] N. P. Belfiore, G. B. Broggiato, M. Verotti, R. Crescenzi, M. Balucani, A. Bagolini, P. Bellutti, M. Boscardin, Development of a MEMS technology CSFH based microgripper, Proc. of the 2014 23rd International Conference on Robotics in Alpe-Adria-Danube Region (RAAD), Smolenice, Slovakia, 3 – 5 September 2014. DOI: 10.1109/RAAD.2014.7002273

[31] T. S. Yallew, N. P. Belfiore, A. Bagolini, M. F. Pantano, Performance Analysis of a CSFH-Based Microgripper: Analytical Modeling and Simulation, Micromachines 25 (2022). DOI: 10.3390/mi13091391

[32] F. Vurchio, G. Bocchetta, G. Fiori, A. Scorza, N. P. Belfiore, S. A. Sciuto, A preliminary study on the dynamic characterization of a MEMS microgripper for biomedical applications, Proc. of the

2021 IEEE International Symposium on Medical Measurements and Applications (MeMeA), Lausanne, Switzerland, 23 – 25 June 2021.
DOI: 10.1109/MeMeA52024.2021.9478703

[33] N. P. Belfiore, A. Bagolini, A. Rossi, G. Bocchetta, F. Vurchio, R. Crescenzi, A. Scorza, P. Bellutti, S. A. Sciuto, Design, Fabrication, Testing and Simulation of a Rotary Double Comb Drives Actuated Microgripper, Micromachines 12 (2021).
DOI: 10.3390/mi12101263

[34] G. Bocchetta, G. Fiori, A. Scorza, N. P. Belfiore, S. A. Sciuto, First results on the functional characterization of two rotary comb-drive actuated MEMS microgripper with different geometry, Proc. of the 25th IMEKO TC4 Symp. and 23nd Int. Workshop on ADC and DAC Modelling and Testing (IWADC), Brescia, Italy, 12 – 14 September 2022.
DOI: 10.21014/tc4-2022.28

[35] F. Vurchio, G. Fiori, A. Scorza, S. A. Sciuto, Comparative evaluation of three image analysis methods for angular displacement measurement in a MEMS microgripper prototype: A preliminary study, Acta IMEKO 10 (2021) 2, pp. 119-125.
DOI: 10.21014/acta_imeko.v10i2.1047

[36] G. Bocchetta, G. Fiori, F. Filippi, P. Ursi, S. A. Sciuto, A. Scorza, First results on torque estimation by FEA and experimental analysis in a novel CSFH-based microgripper, Proc. of the 26th IMEKO TC4 Symp. and 24th Int. Workshop on ADC and DAC Modelling and Testing (IWADC), Pordenone, Italy, 20 – 21 September 2023.
DOI: 10.21014/tc4-2023.42

[37] Y. Wei, Q. Xu, An overview of micro-force sensing techniques, Sens. Actuators A Phys. 234 (2015), pp. 359-374.
DOI: 10.1016/j.sna.2015.09.028

[38] S. A. Bazaz, N. Abbas, M. Bilal Saif, N. Ahmad, Design and characterization of MEMS based micrograsping system. Assem. Autom. 33 (2013), pp. 260-271.
DOI: 10.1108/AA-12-2013-072

[39] R. Cecchi, M. Verotti, R. Capata, A. Dochshanov, G. B. Broggiato, R. Crescenzi, M. Balucani, S. Natali, G. Razzano, F. Lucchese, A. Bagolini, P. Bellutti, E. Sciubba, N. P. Belfiore, Development of micro-grippers for tissue and cell manipulation with direct morphological comparison, Micromachines 6 (2015), pp. 1710-1728.
DOI: 10.3390/mi6111451

[40] N. P. Belfiore, M. Verotti, R. Crescenzi, M. Balucani, Design, optimization and construction of MEMS-based micro grippers for cell manipulation, Proc. of the 2013 International Conference on System Science and Engineering (ICSSE), Budapest, Hungary, 4 – 6 July 2013.
DOI: 10.1109/ICSSE.2013.6614642

[41] A. Bagolini, S. Ronchin, P. Bellutti, M. Chistè, M. Verotti, N. P. Belfiore, Fabrication of Novel MEMS Microgrippers by Deep Reactive Ion Etching With Metal Hard Mask, J. Microelectromech. Syst. 26 (2017), pp. 926-934.
DOI: 10.1109/jmems.2017.2696033

[42] T. Chen, L. Sun, L. Chen, W. Rong, X. Li, A hybrid-type electrostatically driven microgripper with an integrated vacuum tool. Sens. Actuators A Phys. 158 (2010), pp. 320-327.
DOI: 10.1016/j.sna.2010.01.001

[43] Y. S. Oh, W. H. Lee, H. E. Stephanou, G. D. Skidmore, Design, optimization, and experiments of compliant microgripper, in Proc. of the ASME 2003 International Mechanical Engineering Congress and Exposition. Microelectromechanical Systems. Washington, DC, USA, 15 – 21 November 2003.
DOI: 10.1115/IMECE2003-55013

[44] G. Bocchetta, G. Fiori, A. Scorza, S. A. Sciuto, Image quality comparison of two different experimental setups for MEMS actuators functional evaluation: a preliminary study, Proc. of the 25th IMEKO TC4 Symp. and 23nd Int. Workshop on ADC and DAC Modelling and Testing (IWADC), Brescia, Italy, 12 – 14 September 2022.
DOI: 10.21014/tc4-2022.59

[45] M. De Cecco, A. Luchetti, M. Tavernini, Monte Carlo human identification refinement using joints uncertainty, Acta IMEKO 12 (2023) 2, pp. 1-11.
DOI: 10.21014/actaimeko.v12i2.1423

[46] W. M. Zhang, H. Yan, Z. K. Peng, G. Meng, Electrostatic pull-in instability in MEMS/NEMS: A review, Sens. Actuators A Phys. 214 (2014), pp. 187-218.
DOI: 10.1016/j.sna.2014.04.025

[47] M. A. Hopcroft, W. D. Nix, T. W. Kenny, What is the young's modulus of silicon?, J. Microelectromech. Syst. 19 (2010), pp. 229-238.
DOI: 10.1109/jmems.2009.2039697

[48] A. Masolin, P. O. Bouchard, R. Martini, M. Bernacki, Thermo-mechanical and fracture properties in single-crystal silicon, J. Mater. Sci. 48 (2013), pp. 979-988.
DOI: 10.1007/s10853-012-6713-7

[49] B. Bhushan, X. Li, Micromechanical and tribological characterization of doped single-crystal silicon and polysilicon films for microelectromechanical systems devices, J. Mater. Res. 12 (1997), pp. 54-63.
DOI: 10.1557/JMR.1997.0010

[50] J. Liu, N. A. Abu Osman, M. Al Kouzbary, H. Al Kouzbary, N. A. Abd Razak, H. N. Shasmin, N. Arifin, Stiffness estimation of planar spiral spring based on Gaussian process regression, Sci. Rep. 12 (2022), pp. 1-15.
DOI: 10.1038/s41598-022-15421-1

[51] P. Ursi, A. Rossi, F. Botta, N. P. Belfiore, Analytical Modeling of a New Compliant Microsystem for Atherectomy Operations, Micromachines 13 (2022), pp. 1094-1123.
DOI: 10.3390/mi13071094

[52] J. R. Taylor, An introduction to Error Analysis: The study of Uncertainties in Physical Measurements, University Science Books, New York, 1997, ISBN: 9780935702422.

[53] P. N. Prasad, Introduction to Biophotonics, John Wiley & Sons, Hoboken, 2003. ISBN: 9780471287704.

[54] G. Fiori, G. Bocchetta, S. Conforto, S. A. Sciuto, A. Scorza, Sample volume length and registration accuracy assessment in quality controls of PW Doppler diagnostic systems: a comparative study, Acta IMEKO 12 (2023) 2, pp. 1-7.
DOI: 10.21014/actaimeko.v12i2.1425

[55] N. Covre, A. Luchetti, M. Lancini, S. Pasinetti, E. Bertolazzi, M. De Cecco, Monte Carlo-based 3D surface point cloud volume estimation by exploding local cubes faces, Acta IMEKO 11 (2022) 2, pp. 1-9.
DOI: 10.21014/acta_imeko.v11i2.1206

[56] G. Fiori, A. Pica, S. A. Sciuto, F. Marinozzi, F. Bini, A. Scorza, A comparative study on a novel quality assessment protocol based on image analysis methods for color Doppler ultrasound diagnostic systems, Sensors 22 (2022).
DOI: 10.3390/s22249868

[57] T. Tillocher, J. Nos, G. Antoun, P. Lefaucheux, M. Boufnichel, R. Dussart, Comparison between Bosch and STiGer Processes for Deep Silicon Etching, Micromachines 12 (2021).
DOI: 10.3390/mi12101143

[58] T. Xu, Z. Tao, H. Li, X. Tan, H. Li, Effects of deep reactive ion etching parameters on etching rate and surface morphology in extremely deep silicon etch process with high aspect ratio, Adv. Mech. Eng. 9 (2017).
DOI: 10.1177/1687814017738152

[59] B. Nöhammer, C. David, H. Rothuizen, J. Hoszowska, A. Simionovici, Deep reactive ion etching of silicon and diamond for the fabrication of planar refractive hard X-ray lenses, Microelectron. Eng. 67-68 (2003), pp. 453-460.
DOI: 10.1016/S0167-9317(03)00101-1

[60] M. Huff, Recent advances in reactive ion etching and applications of high-aspect-ratio microfabrication, Micromachines 12 (2021).
DOI: 10.3390/mi12080991

[61] M. Verotti, P. Di Giamberardino, N. P. Belfiore, O. Giannini, A genetic algorithm-based method for the mechanical characterization of biosamples using a MEMS microgripper:

numerical simulations, J. Mech. Behav. Biomed. Mater. 96 (2019), pp. 88-95.
DOI: 10.1016/j.jmbbm.2019.04.023

[62] Y. Yu, W. Yang, B. Wang, M. A. Meyers, Structure and mechanical behavior of human hair, Mater. Sci. Eng. C 73 (2017), pp. 152-163.
DOI: 10.1016/j.msec.2016.12.008

[63] Z. Hu, G. Li, H. Xie, T. Hua, P. Chen, F. Huang, F, Measurement of Young's modulus and Poisson's ratio of human hair using optical techniques. Proc. of SPIE Fourth International Conference on Experimental Mechanics, Singapore, Singapore, 18 – 20 November 2009.

[64] O. Baer, C. Giusca, R. Kumme, A. Prato, J. Sander, D. Mirian, F. Hauschild, Digital Twin concept of a force measuring device based on the finite element method, Acta IMEKO 12 (2023)1, pp. 1-5.
DOI: 10.21014/actaimeko.v12i1.1404